

Supporting information

Nanoscale dynamics of phospholipids reveals optimal assembly mechanism of pore-forming proteins in bilayer membranes

Nirod Kumar Sarangi, K. G. Ayappa, Sandhya. S. Visweswariah, and Jaydeep Kumar Basu

Surface pressure-area isotherm and layer-by-layer phospholipid monolayer transfer for fabrication of SLBs: Surface pressure versus area-per-molecule isotherms were recorded using the KSV LB rectangular mini Trough (area, 240 cm²) equipped with a Wilhelmy balance. A platinum sensor of accuracy 0.1 mN/m was used to measure the interfacial surface pressure. A chloroform solution of either one component DOPC, POPC and DMPC lipid or binary mixture containing varied cholesterol content such as 3:1, 2:1 and 1:1 were spread on the air–water interface of a LB trough at 20 °C using a precise Hamilton syringe to make a compact monolayer. After evaporation of chloroform, the isotherms were recorded at constant temperature and a barrier speed of 5 mm/min.

Figure S1 shows the pressure-area isotherm of pristine DOPC, POPC and DMPC monolayers and with lipid to cholesterol ratios ranging from 3:1, 2:1 and 1:1. The mean molecular areas for DOPC, POPC and DMPC are ~85, 73 and 55 Å²/molecule respectively. The decrease in mean molecular area is due to a decrease in hydration of the head group and higher van der Waals interaction among the alkyl chains. Upon addition of 25% cholesterol in the respective monolayers, the mean molecular area further decreases due to the condensing effect of cholesterol. At higher percentage of cholesterol such as 33 (2:1) and 50% (1:1), the mean molecular area increases more gradually suggesting higher orderd structures and possible domain formation. The condensing effect of cholesterol is due to the intermolecular cooperative interaction between the cholesterol –OH groups and lipid head groups and degree of rigidity of the monolayer. Our results also further supported by the maximum compressibility coefficient $C_s = -\left(\frac{1}{A}\right)\left(\frac{\delta A}{\delta \pi}\right)$ data as shown in Figs. S1 b, d and f.

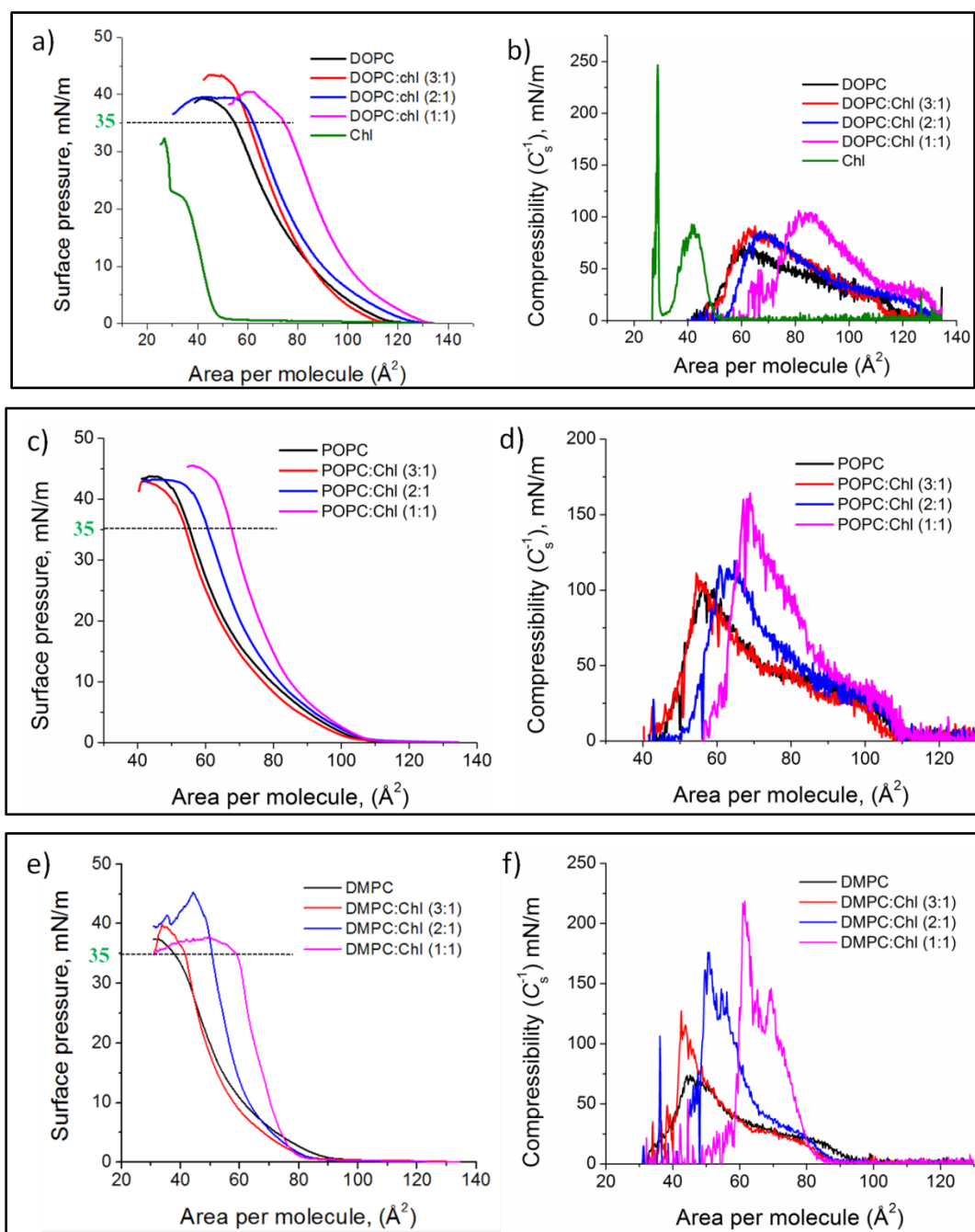


Figure S1. Panel (a), (c) and (e) illustrate surface pressure-area isotherms of pristine (a) DOPC, (b) POPC and (c) DMPC, and with lipid to cholesterol ratio of 3:1, 2:1 and 1:1 respectively at 20 °C. The supported lipid bilayers bilayers were prepared at highly condensed surface pressure of 35 mN/m as marked in horizontal dotted line. Right panels show the compressibility plots of the respective monolayers derived from the π -A data.

Supported lipid bilayers were formed upon controlled transfer of lipid interfacial monolayers onto pre-treated glass substrates by employing the Langmuir-Blodgett (LB) method. During the preparation of bilayers using the LB method, multiple compression-expansion cycles were followed before the collapse surface pressure and subsequently the bilayers were transferred at a highly condensed surface pressure of 35 mN/m to the hydrophilized glass slides by using layer-by-layer transfer. Prior to transfer, glass substrates (20 mm×20 mm, Germany) were cleaned using “piranha solution” (a 30:70 mixture of 30% hydrogen peroxide and concentrated sulfuric acid at 80 °C) for 30 min and washed multiple times with MilliQ DI water (resistivity \approx 18.2 M Ω .cm). The first monolayer was transferred at an equilibrium pressure of 35 mN/m by vertical withdrawal of the substrate at a speed of 5 mm/min with a transfer ratio of \sim 1.2 \pm 0.1. In the monolayer transferred onto the hydrophilic glass surface, the charged head groups of lipid faced the glass surface and the hydrophobic hydrocarbon chains were directed towards the air. The second monolayer transfer at the same surface pressure by a vertical down stroke yielded a centro-symmetric bilayer (Y-type) on the support. To make the bilayer luminescent, dye tagged lipid (Atto488PE, 10⁻⁴ mol%) was mixed thoroughly with pristine DOPC or DOPC:Chl before spreading at the air-water interface. After transfer, the bilayers were transferred to a container under water and stored at room temperature for further use. All measurements were done within 24 hours of the LB transfer.

Atomic force microscopy:

Figures S2 a-c shows the topographic images for DOPC:Chl, POPC:Chl and DMPC:Chl pristine SLBs prior to incubating with Listeriolysin O (LLO). The bottom panel of the respective images shows the line profile analyses as marked in the figures. In all the cases, the bilayers are prepared by using LB technique and images were acquired under liquid. Our AFM images of the pristine bilayer are homogeneous in nature devoid of any phase coexistence. The selected regions presented here illustrate parts of the bilayers where we identified the presence of defects in order to determine the bilayer heights with respect to the glass substrate. Figure S2d represents the 3D view of the aggregate structures such as pores, arcs and coalesced pores after incubation of LLO in the DOPC:Chl SLBs. Figure S2e depicts the control experiment, where the LLO free DOPC:Chl bilayer was incubated at 37 °C *off-situ* and then transferred to the liquid cell for

imaging. The absence of any aggregate like structures confirms that the observed structures as shown in Fig.S2d are formed solely due to LLO toxin binding and oligomerization.

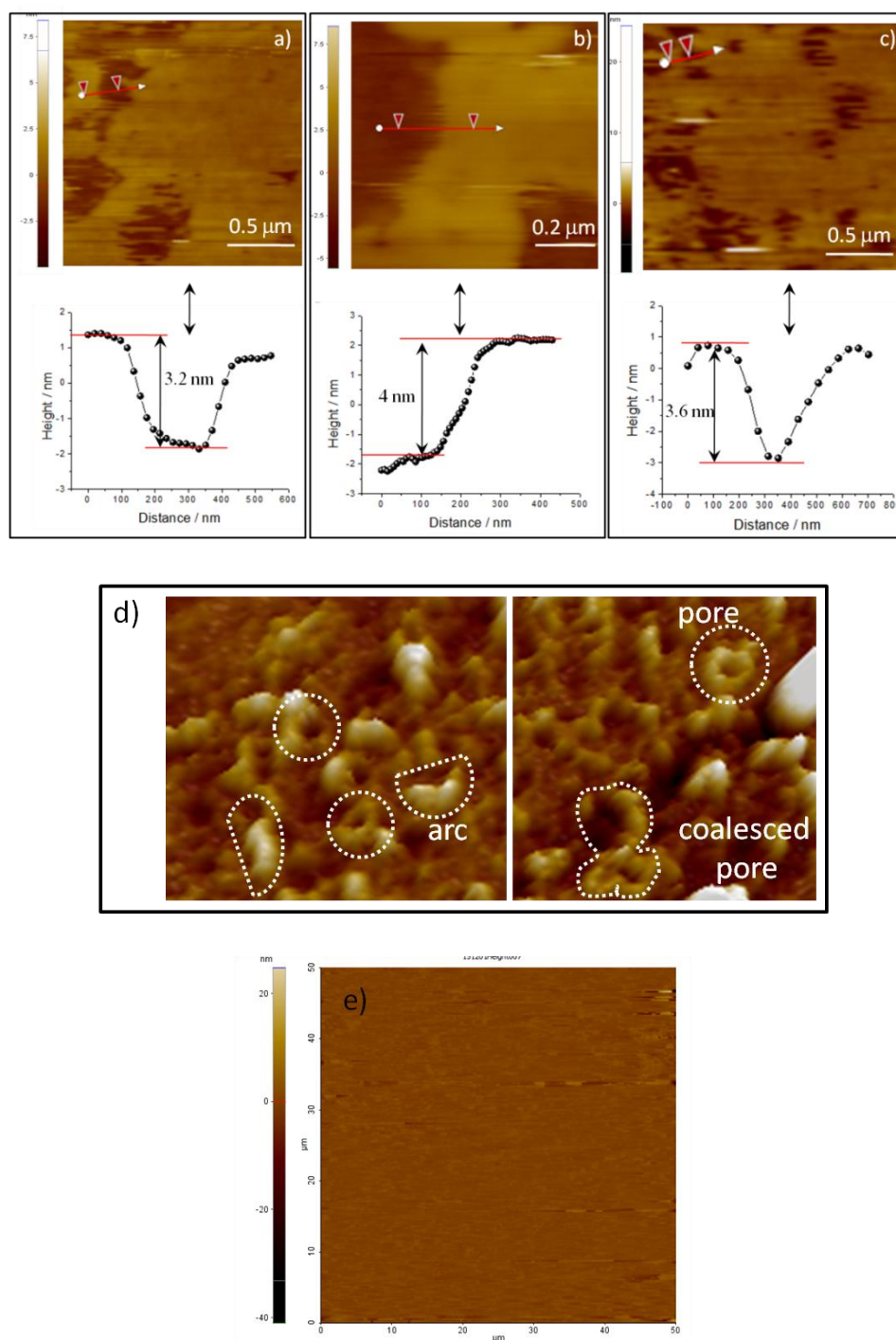


Figure S2. a) AFM image of (a) DOPC:Chl, (b) POPC:Chl and (c) DMPC:Chl bilayer before LLO incubation. In all the bilayers, the cholesterol concentration was 25% and were transferred

by LB method. Bottom panel shows the line profile analyses of the respective images. (d) represents the 3D view of the selective regions showing pore, arc and coalesced pore after LLO incubation of DOPC:Chl SLBs. (e) Represents the control experiment, where the DOPC:Chl bilayer was incubated at 37 °C in the absence of LLO toxin showing absence of any aggregate like structures.

STED-FCS Nanoscope

For imaging and FCS, we applied STED-FCS nanoscopy using a commercial STED setup (SP5x, Leica Microsystems GmbH, Mannheim, Germany). Ar ion laser and a STED laser (592 nm) with a continuous-wave (CW) mode were aligned in such a way to accomplish a doughnut-shaped focal intensity distribution featuring a central zero intensity and a diffraction-unlimited spot. The master power of the Ar laser was set to 25-30% and subsequently excitation at 488 nm was used at 1–25% output power. The CW-STED 592 nm laser was operated at 0–100% output power (varying in the range 0–260 mW measured directly at the focal plane of a 10X air objective). Before each series of measurements the auto-alignment procedure (super-imposing the excitation laser and the depletion lasers) was performed in 25 nm×25 nm pixel area. This procedure was repeated every 15 minutes. An oil immersion objective, 100x 1.4 NA is used for focusing of the superimposed excitation and STED laser beams as well as collection of the fluorescence emitted intensity. The emitted intensity was guided to the microscope objective back aperture through the confocal pinhole (set to 1 Airy unit) filtered by a 594 nm notch filter imaged onto a single-photon-counting avalanche photo-diode (APD; Micro Photon Devices, PicoQuant, Berlin, Germany) in the external port of the microscope with a band-pass filter (BS 560) between 500–550 nm.

Analyses of STED-FCS:

The advent of STED fluorescence microscopy can reduce the detection volume to many fold (< 100 nm) by suppressing the fluorescence excitation at the outer part of the focal spot (Fig. S5a). The recorded fluorescence bursts considered as single molecule time trace of dye tagged lipid molecules crossing the typical confocal and STED volume are shown in Fig. S5b. The corresponding intensity-intensity correlation raw and normalized data accrued from confocal and

STED recordings are shown in Figures S5 c and d respectively. In STED-FCS, the amplitude was higher and lag time reduces when compared to that of regular confocal FCS.

The particle number fluctuations $N(t) = \langle N \rangle + \delta N(t)$ of fluorescent molecules entering and leaving the focus of a confocal microscope during the excitation can be calculated by measuring the emitted intensity $I(t)$ as $I(t) = \langle I \rangle + \delta I(t)$; where $\langle I \rangle$ and $\delta I(t)$ represents a time averaged intensity and fluctuations respectively. In FCS, the autocorrelation function $G(t_c)$ from the intensity signal $I(t)$ measured in the microscope is calculated using;

$$G(t_c) = \frac{\langle \delta I(t) \cdot \delta I(t+t_c) \rangle_t}{\langle I(t) \rangle_t^2} \quad (\text{S1})$$

where $\langle \dots \rangle_t$, denotes a time average over the time variable t .

The values of the spot diameter d in confocal mode used throughout our calculation for estimating the diffusion coefficient D were found to be ~ 200 nm (at 100X, oil immersion objective) and was obtained from the point spread function (PSF) by scanning fluorescent chromeo 488 beads of 40 nm size. For calibration of the diameters of the effective focal spot ($d_{P_{STED}}$) created by different STED powers (P_{STED}), we performed STED-FCS measurements of Atto488 DPPE (PE) fluorescent analogues stained in both leaflets of the pristine DOPC supported lipid bilayers prepared by the LB method. At STED power zero (or in normal confocal mode), the d ($P_{STED} = 0$) and the other effective diameters at different STED power d ($P_{STED} \neq 0$) can be obtained using equation S2;

$$\frac{d(P_{STED}=0)}{d(P_{STED})} = \sqrt{\frac{\tau_D(P_{STED}=0)}{\tau_D(P_{STED})}} \quad (\text{S2})$$

where τ_D is the transit times correspond to each values of STED power used. In the above equation we assume that the lipid diffusion in pristine DOPC SLBs undergoes a two dimensional free Brownian diffusion where the diffusion time scales with the diffusion area.

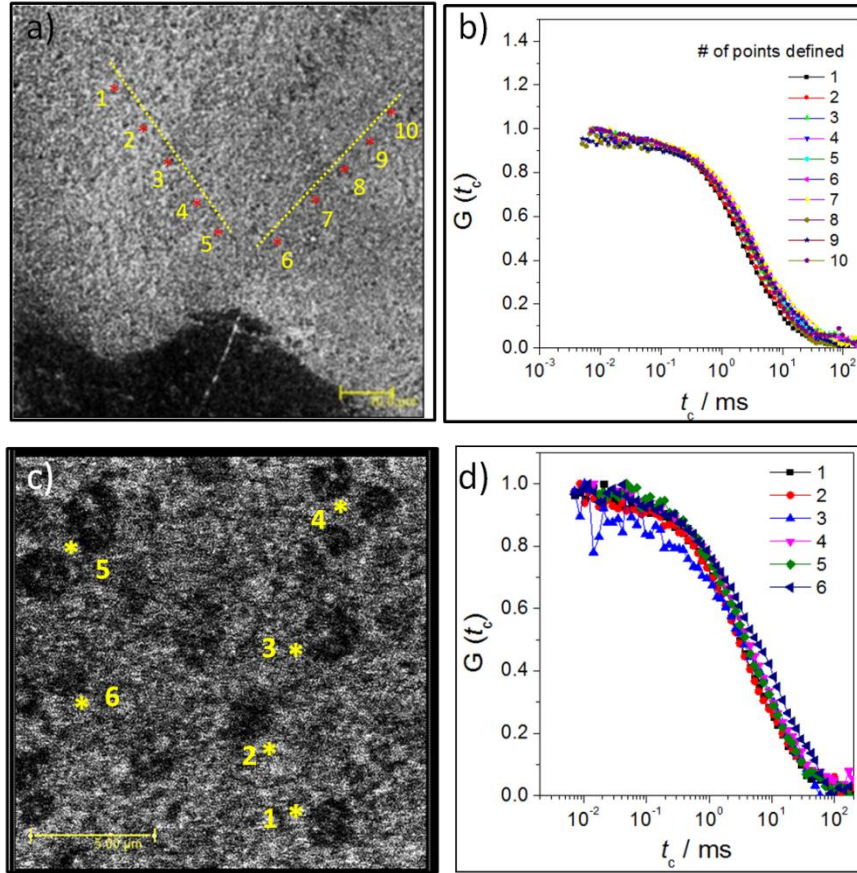


Figure S3. Confocal microscopy image of DOPC:Chl (3:1) SLBs (a) before and (c) after LLO incubation. b) and d) represents normalized correlation data recorded in the different locations marked in the respective figures (a) and (c) respectively.

Diffusing wave spectroscopy: Diffusing wave spectroscopy (DWS) [Rheolab II, LS Instruments] based microrheology (MR) measurements were performed DMPC:Chl SUVs similar to the measurements discussed earlier [1]. Experiments were carried on these samples by using 1 mm thick glass cuvette and 687 nm incident laser line for scattering and the data were collected in transmission mode. The temperature of the sample was varied from 16 to 45 °C in steps of 2° to study the effect of LLO (0.086 μM) binding on the dynamics and phase behavior of the SUVs. LLO incubation was done at 37 °C for 30 min in an Eppendorf. At each temperature, data were collected after thermally stabilizing the system. Using the intensity-intensity auto correlation function $g_2(t)$ we have estimated the half life time (t_1), by using ;

$$g_2(t) = g_0 + A_1 e^{\left(\frac{-t}{t_1}\right)} \quad (\text{S3})$$

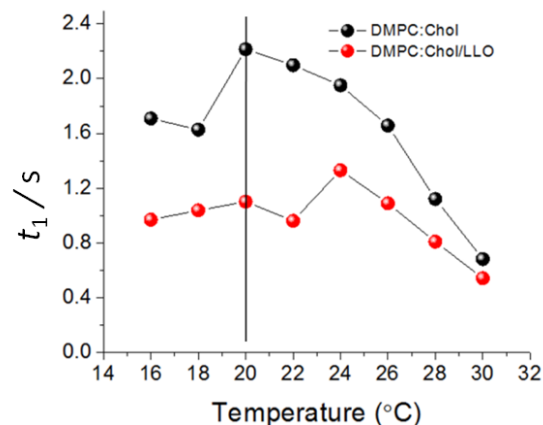


Figure S4. Variation of half life resident time with temperature for DMPC:Chl SUVs before (black filled circle) and after (red filled circle) LLO incubation lipid vesicles. The vertical line with maxima denotes the shift of fluid–gel transition temperature after incubation.

Here, half life time (t_1) denotes the residence time of photons before being transmitted from the cuvette. Half time was calculated by fitting the normalized autocorrelation intensity values to equation S3. When the lipids are in transition phase, the lipid reorganizes itself causing temporal fluctuations in the scattered light intensity which in turn increases the path length of a single photon. Hence the intensity fluctuations, when correlated will give a slower decay i.e., increased half time. Only during the transition phase, this phenomenon can be observed. From the plot, the temperature corresponding to the peak i.e., larger t_1 , represents the transition temperature of the lipid used. The results depicted above in Fig. S4 shows a shift in the transition temperature of the DMPC:Chl lipids in SUVs when added with LLO. The shift towards higher temperature indicated that the lipids were in ordered state at room temperature and diffusion of lipids is related to the ordered nature of the lipids.

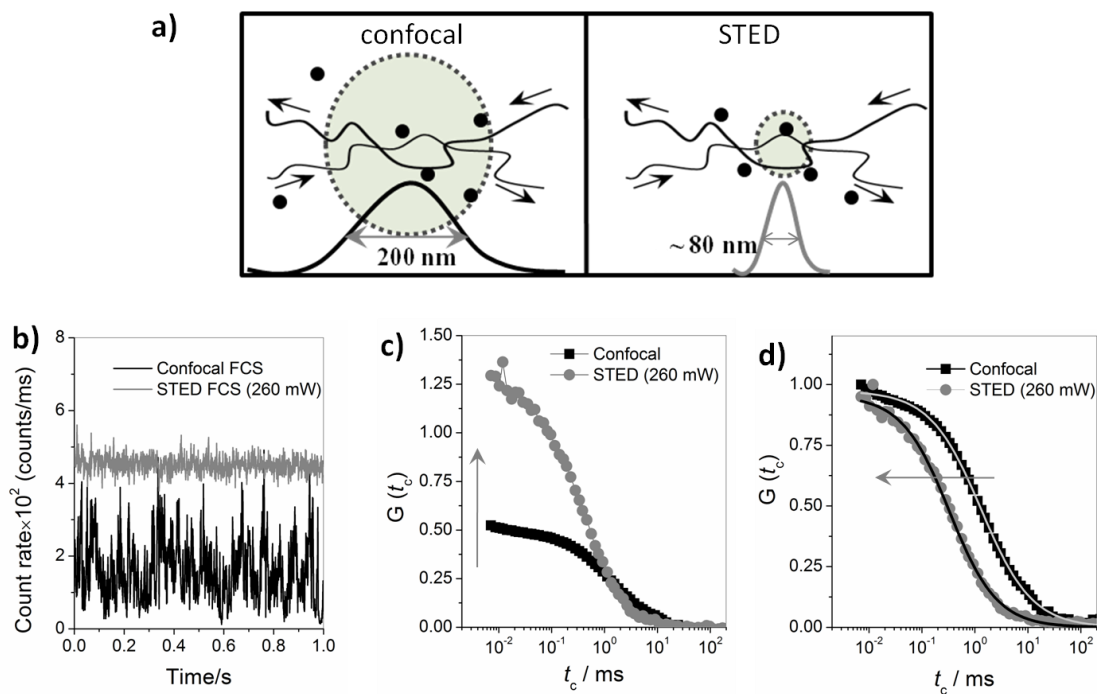


Figure S5. Schematic diagram (redrawn from reference [2]) showing the diffusion of fluorescent PE molecules across the plane of DOPC:Chl bilayer membrane in diffraction limited confocal detection area (diameter, $d = 200$ nm) created by excitation laser and diffraction unlimited detection area (diameter, $d = 80$ nm) created by superimposing 592 STED laser with the exciting laser. (b) Shows fluorescence signal bursts from PE diffusing in DOPC:Chl bilayers membrane detected with a confocal (black line) and STED (grey line) spot. (c) and (d) represents the raw and normalized intensity-intensity correlation data accrued from confocal and STED recordings.

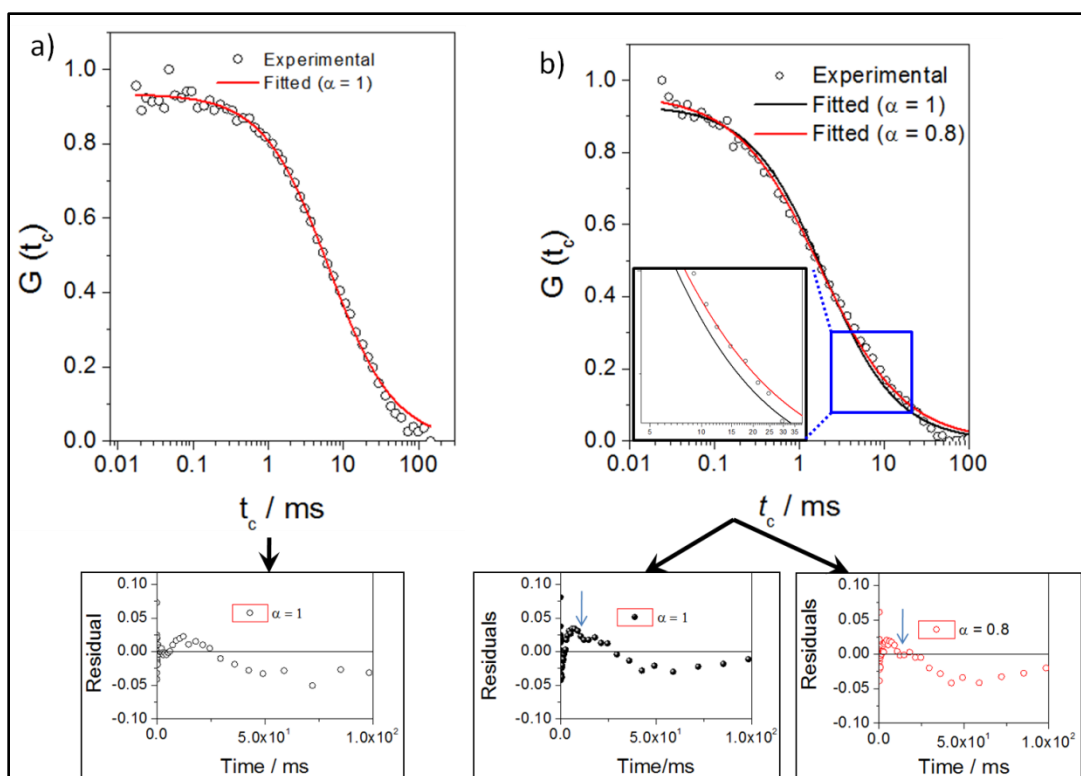


Figure S6. (a) and (b) represents normalized correlation data of POPC:Chl bilayer after LLO incubation recorded at before (low STED power or high PSF or high focal spot area) and after (high STED power or low PSF or low focal spot area) the cross over regime. At high focal spot area, irrespective of the model whether free diffusion (where, $\alpha=1$ was fixed in Eq. 1 during the fit, see solid red line in Fig. S6a) or anomalous diffusion model (extracted α was found to be 1.02, fit not shown), the transit time ($\tau_D \sim 6.3$) values did not change significantly. In contrast, at low focal spot area, a better fit as shown in Fig. S6b (red line inset), was obtained for anomalous diffusion model ($\tau_D = 1.77$ and $\alpha=0.8$) than the free diffusion model ($\tau_D = 1.96$ and $\alpha=1$). The confidence limit for all the fit was $R^2 > 0.99$. Bottom panel represents the residuals of the free diffusion and anomalous diffusion model fit as shown in Figs. S6 a and b respectively, showing the accuracy of the fit.

Reference:

1. Weitz DA, Zhu JX, Durian DJ, Gang HU, Pine, DJ, *Phys. Scr.* **1993**, T49B, 610.
2. Eggeling C, Ringemann C, Medda R, Schwarzmann G, Sandhoff K, Polyakova S, Belov VN, Hein B, von Middendorff C, Schönle A, Hell SW, *Nature*, **2009**, 457, 1159.